# Development and Field Evaluation of a Solar-Powered LoRa-Based Air Quality Monitoring and Early-Warning System for a Sand-Mining Area

**Alamsyah[1*], Aidynal Mustari[2], Moh. Ikro Fajar Rahman[3], Mohammed Ikhlayel[4]**
[1,2,3]Department of Electrical Engineering, Faculty of Engineering, Tadulako University, Palu, Indonesia
[4]Department of Information Technology and Communications, Al-Quds Open University, Ramallah 51000, Palestine

**Article Info**

***Article history:***

Received August 23, 2026
Revised August 30, 2026
Accepted September 03, 2026

***Keywords:***

air quality monitoring
LoRa
sensor
solar-powered system
web server

**ABSTRACT**

Air pollution generated by sand-mining activities can degrade environmental quality and increase public-health risks, particularly in locations lacking continuous air-quality monitoring infrastructure. This study presents the development and field evaluation of a solar-powered LoRa-based air-quality monitoring and early-warning system for the Watusampu sand-mining area in Palu City, Indonesia. The proposed system integrates autonomous solar power, long-range wireless communication, multi-parameter sensing, real-time visualization, local backup storage, and Indonesia's Air Pollutant Standard Index (ISPU)-based warning functions. The transmitter node combines ZH03B, MiCS-5524, and DHT22 sensors with an ESP32 and an RFM95W LoRa module to measure $PM_1$, $PM_{2.5}$, $PM_{10}$, carbon monoxide, temperature, and relative humidity. The receiver processes and stores the measurements on a microSD card, uploads them to a web database, and displays them through an LCD and web dashboard. Air-quality status is determined according to the highest ISPU sub-index for $PM_{2.5}$, $PM_{10}$, and CO. Sensor performance was evaluated by comparison with a reference instrument, while LoRa communication was tested under line-of-sight (LoS) and non-line-of-sight (NLoS) conditions. The ZH03B sensor produced mean relative errors of 6.61%, 10.58%, and 8.67% for $PM_1$, $PM_{2.5}$, and $PM_{10}$, respectively. The MiCS-5524 sensor produced a mean relative error of 18.48% for CO, while the DHT22 produced mean relative errors of 0.87% for temperature and 0.61% for relative humidity. LoRa communication achieved 0% packet loss up to 1.2 km under LoS conditions and up to 20 m under the tested NLoS conditions. These findings demonstrate the technical feasibility of the proposed platform for short-term indicative air-quality monitoring and local early warning in sand-mining areas with limited infrastructure.



***Corresponding Author:***
Alamsyah
Department of Electrical Engineering, Faculty of Engineering, Tadulako University, Palu, Jl. Soekarno Hatta No. KM. 9, Tondo, Kec. Mantikulore, Kota Palu, Sulawesi Tengah ,94148), Indonesia.
Email: alamsyah.zakaria@untad.ac.id ; Orchid ID: https://orcid.org/0009-0003-9452-1594

## 1. INTRODUCTION

Air pollution is a major environmental and public-health concern worldwide [1], [2]. Rapid urbanization [3]–[5], industrial activities, transportation emissions [6], and fossil-fuel combustion have increased ambient concentrations of harmful pollutants. Particulate matter (PM) [7] and carbon monoxide (CO) [8] are particularly important because prolonged exposure is associated with respiratory and cardiovascular disorders. Ambient temperature and relative humidity are not pollutants but relevant meteorological parameters because they influence pollutant formation, dispersion, and sensor response. Continuous monitoring of these variables is therefore essential for assessing air-quality conditions and supporting timely risk mitigation.

Conventional air-quality monitoring stations can provide accurate and standardized data, but their high installation and maintenance costs restrict deployment density, especially in remote or infrastructure-limited areas. Low-cost sensors combined with Internet of Things (IoT) platforms have therefore become a practical option for distributed and real-time air-quality monitoring [9], [10]. However, their use in field conditions is still affected by measurement uncertainty, environmental disturbances, calibration needs, limited power supply, and reliance on communication technologies with restricted range or relatively high energy consumption. LoRa can help overcome some of these constraints by supporting low-power transmission of small environmental data packets over long distances [11]–[13]. Despite this advantage, many existing LoRa-based monitoring studies still focus mainly on prototype functionality or data visualization, with limited combined evaluation of sensor accuracy, communication reliability under different propagation conditions, autonomous power operation, and regulation-based early-warning capability in an active pollution-source environment.

Sand-mining and quarrying operations can generate particulate emissions through excavation, crushing, loading, stockpiling, and material transportation. Heavy equipment and fossil-fuel-powered vehicles may also contribute combustion-related pollutants, including carbon monoxide [14], while temperature and relative humidity can affect pollutant dispersion and the response of low-cost sensors [15]. Watusampu was selected as the field site because it is a documented sand- and stone-mining area along the Palu–Donggala corridor, where mining has been associated with reported environmental and community-health concerns. An earlier assessment of Watusampu described mining in lowland, upland, and river areas and reported damage to agricultural land, riverbanks, and roads, together with health concerns [16]. More recent research at Watusampu and the adjacent Palu–Donggala mining corridor reported elevated or variable $PM_{2.5}$ and $PM_{10}$ concentrations and identified mining activity as a relevant source requiring air-quality assessment [17], [18].

Accordingly, this study develops and field-evaluates a solar-powered LoRa-based system for monitoring $PM_1$, $PM_{2.5}$, $PM_{10}$, CO, temperature, and relative humidity in the Watusampu sand-mining area. The platform integrates autonomous power supply, multi-parameter sensing, long-range data transmission, local and web-based storage, real-time visualization, and an early-warning mechanism based on Indonesia's Air Pollutant Standard Index (ISPU), as regulated by Minister of Environment and Forestry Regulation No. 14 of 2020. The warning status is determined from the highest ISPU subindex calculated for $PM_{2.5}$, $PM_{10}$, and CO, with alerts triggered when the air-quality category reaches Unhealthy or higher. System performance was evaluated through comparison with a reference instrument, LoRa communication tests under Line-of-Sight and Non-Line-of-Sight conditions, and a seven-day field deployment. This study provides practical evidence regarding the feasibility and limitations of an integrated low-cost monitoring platform for pollution-prone areas with limited infrastructure.

Previous studies have evaluated low-cost air-quality sensors using co-location with reference instruments, calibration equations, regression models, and error metrics such as mean absolute error, root-mean-square error, and correlation coefficients [19]-[22]. These approaches are useful for determining whether a sensor can support indicative monitoring, but their results are difficult to compare when the reference method, co-location period, sampling frequency, environmental conditions, calibration procedure, and number of paired observations are not reported consistently [23]. In addition, sensor validation is often conducted separately from communication and power-system evaluation [24]. A field study that reports these elements together can therefore provide a more complete assessment of deployment readiness, while still distinguishing technical feasibility from regulatory measurement equivalence [25].

Environmental monitoring systems commonly use Wi-Fi, GSM, or cellular networks for data transmission; however, their effectiveness depends on infrastructure availability, communication range, required data rate, and power consumption. Wi-Fi can support higher data rates but is constrained by short transmission distance and the need for nearby access points. Cellular networks provide broader coverage, yet they may increase energy demand and operational cost. In comparison, LoRa is intended for long-range, low-data-rate communication in energy-limited applications [26], making it appropriate for periodic transmission of compact sensor data from remote monitoring nodes. However, its actual communication range and reliability are influenced by antenna configuration, radio parameters, terrain conditions, and Line-of-Sight (LoS) availability.

## 2. METHOD

This study adopted a design, implementation, and field-evaluation approach to develop a solar-powered LoRa-based air-quality monitoring and early-warning system. The system measured six environmental parameters: $PM_1$, $PM_{2.5}$, $PM_{10}$, carbon monoxide (CO), ambient temperature, and relative humidity. These parameters were selected to represent particulate and gaseous emissions associated with excavation, material handling, heavy-equipment operation, and transportation activities. Temperature and relative humidity were also monitored because they can affect pollutant dispersion and sensor response. The system was deployed in the Watusampu sand-mining area, Palu City, Central Sulawesi, Indonesia. Evaluation was conducted through three stages: comparison of sensor readings with a reference instrument, LoRa

ISSN: 2715-6427

communication testing under Line-of-Sight and Non-Line-of-Sight conditions, and a seven-day field deployment from 12 to 18 May 2026.

### 2.1. Research Framework

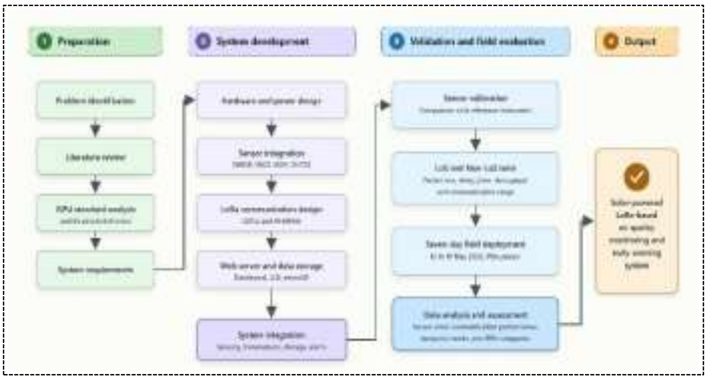


Figure 1. Research framework of the proposed system

Figure 1 presents the research framework, which consists of four stages: preparation, system development, validation and field evaluation, and output. The preparation stage includes problem identification, literature review, analysis of Indonesia's Air Pollutant Standard Index (ISPU), and specification of system requirements. The system-development stage covers hardware and solar-power design, integration of the ZH03B, MiCS-5524, and DHT22 sensors, LoRa communication design, web-server and data-storage development, and full integration of sensing, transmission, storage, visualization, and alarm functions. In the validation and field-evaluation stage, sensor readings are first compared with a reference instrument. LoRa communication is then tested under Line-of-Sight (LoS) and Non-Line-of-Sight (Non-LoS) conditions using packet loss, delay, jitter, throughput, and communication range as performance indicators. The integrated system is subsequently deployed for seven days, from 12 to 18 May 2026, in the Watusampu sand-mining area. The collected data are analyzed to assess sensor error, communication performance, temporal air-quality variation, and ISPU categories. The final output is a solar-powered LoRa-based air-quality monitoring and early-warning system for real-time use in infrastructure-limited sand-mining environments.

### 2.2. System Architecture

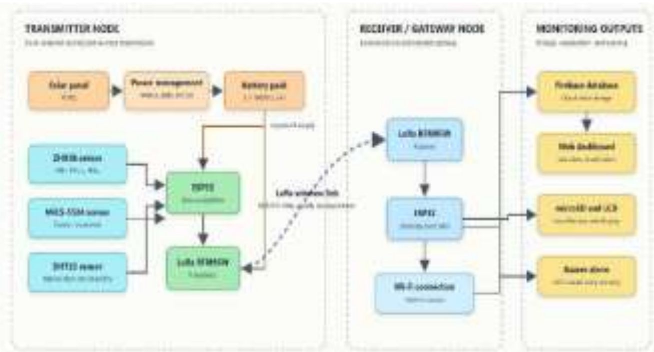


Figure 2. Architecture of the proposed monitoring system

Figure 2 shows the architecture of the proposed system, consisting of a solar-powered transmitter node, a receiver/gateway node, and monitoring outputs. The transmitter node uses ZH03B, MiCS-5524, and DHT22 sensors to measure $PM_1$, $PM_{2.5}$, $PM_{10}$, CO, temperature, and relative humidity. Autonomous operation is supported by a 10 Wp solar panel, a rechargeable battery pack, and a power-management circuit. An ESP32 collects and processes the sensor readings before transmitting the data wirelessly to the receiver through RFM95W LoRa modules. At the receiver/gateway node, another ESP32 receives the data, uploads them to the Firebase database via Wi-Fi, and enables real-time visualization on the web dashboard. The measurements are also displayed on an LCD and stored locally on a microSD card. An ISPU-based buzzer is used to provide early warning when the calculated air-quality category reaches the Unhealthy level or higher.

### 2.3. System Workflow

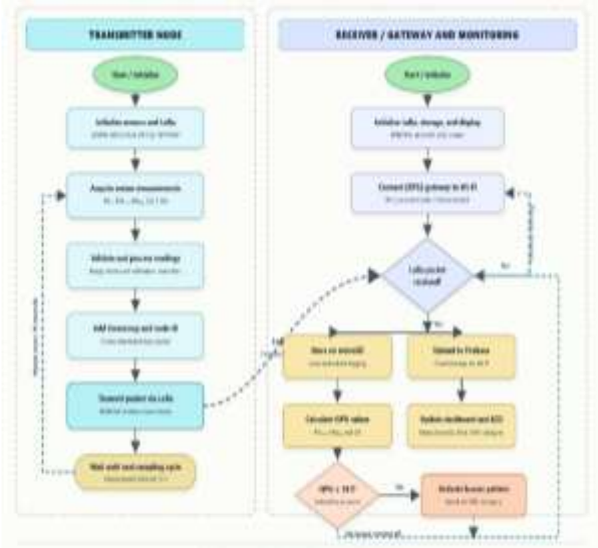

Figure 3. Operational workflow of the proposed monitoring and early-warning system

Figure 3 presents the continuous operational workflow of the proposed system. At the transmitter node, the ZH03B, MiCS-5524, and DHT22 sensors are initialized to measure $PM_1$, $PM_{2.5}$, $PM_{10}$, carbon monoxide (CO), temperature, and relative humidity. The ESP32 acquires the sensor readings, performs range checking and calibration correction, and adds a timestamp and node identifier to each data packet. The packet is then transmitted to the receiver node through the RFM95W LoRa module. This measurement and transmission cycle is repeated every 10 s, regardless of whether the previous packet was successfully received.

At the receiver node, another ESP32 receives and processes the LoRa packet, uploads the data to the Firebase database via Wi-Fi, displays the measurements on the web dashboard and 16 × 2 $I^2C$ LCD, and stores them locally on a microSD card. The system calculates ISPU subindices from $PM_{2.5}$, $PM_{10}$, and CO concentrations, and the highest subindex determines the overall air-quality category. The buzzer remains inactive for Good and Moderate conditions, emits a short warning for Unhealthy conditions, produces a stronger warning for Very Unhealthy conditions, and sounds continuously under Hazardous conditions.

### 2.4. Circuit Schematic

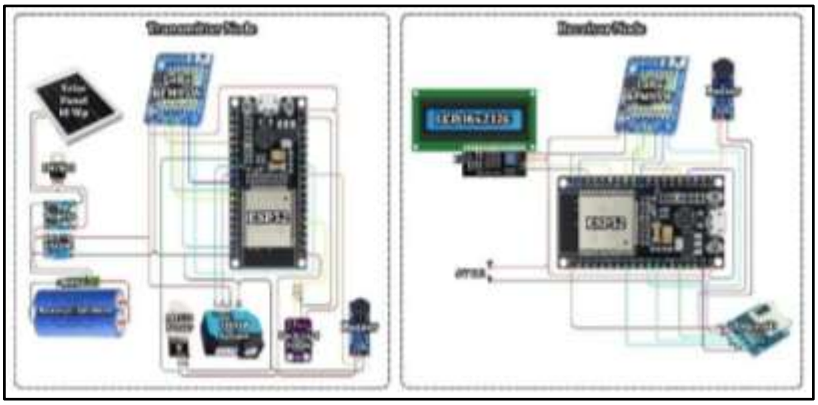

Figure 4. Wiring diagram of the transmitter and receiver nodes

Figure 4 shows the wiring configuration of the transmitter and receiver nodes. The transmitter node is powered by a 10 Wp solar panel, TP4056 charging module, 1S BMS, two 18650 batteries, and an SX1308 step-up converter. Environmental measurements are obtained using the ZH03B sensor for $PM_1$, $PM_{2.5}$, and $PM_{10}$; the MiCS-5524 sensor for CO; and the DHT22 sensor for temperature and relative humidity. The ESP32 processes the sensor data and communicates with the RFM95W LoRa module through the SPI interface, the ZH03B through UART, the MiCS-5524 through an analog input, and the DHT22 through a digital data pin. A buzzer is also included in the transmitter node.

The receiver node uses an adapter as its power source and another ESP32 as the main controller. The RFM95W LoRa module and microSD module are connected through SPI, while the 16 × 2 LCD is connected through the $I_2C$ interface. Received data are uploaded to the Firebase database via Wi-Fi, displayed on the web dashboard and LCD, and stored locally on the microSD card. The receiver node is also equipped with a buzzer for warning indication. Both nodes use a common ground reference to maintain electrical stability.

### 2.5. Hardware Design

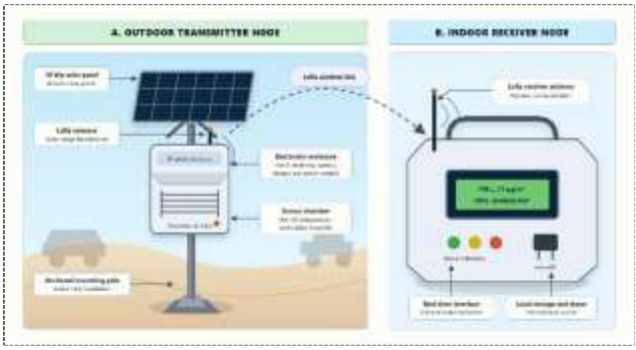

Figure 5. Hardware design of the proposed system

Figure 5 shows the conceptual hardware design of the proposed system, which consists of an outdoor transmitter node and an indoor receiver node. The transmitter node is mounted on an anchored pole to ensure stable installation and sufficient exposure to ambient air at the monitoring site. It integrates a 10 Wp solar panel, a protected electronics enclosure containing the ESP32, RFM95W module, rechargeable battery, and power-management circuit, as well as a weather-shielded sensor chamber for measuring particulate matter, CO, temperature, and relative humidity. The receiver node is installed indoors within Wi-Fi coverage and includes a LoRa antenna, LCD, status indicators, microSD storage, and an ISPU-based buzzer alarm. LoRa antennas on both nodes enable wireless communication between the field transmitter and the receiver gateway. The enclosure and sensor shield reduce direct exposure to sunlight and precipitation while allowing airflow for environmental measurements.

The air-quality alarm mechanism was designed according to Indonesian Minister of Environment and Forestry Regulation No. 14 of 2020 on the Air Pollutant Standard Index (ISPU). This mechanism converts measured pollutant concentrations into warning categories. Individual ISPU subindices are calculated for $PM_{2.5}$, $PM_{10}$, and CO using linear interpolation between the relevant breakpoint values. The highest subindex is then used to determine the overall air-quality category and trigger the corresponding buzzer-warning pattern. The ISPU subindex is calculated using the following equation:

$$I = \frac{(I_a - I_b)}{(X_a - X_b)}(X_x - X_b) + I_b \quad (1)$$

The variables in the ISPU equation can be described as follows: I is the calculated ISPU value; $I_a$ and $I_\beta$ are the upper and lower limits of the relevant ISPU interval; $X_a$ and $X_\beta$ are the upper and lower pollutant-concentration limits corresponding to that interval, expressed in μg/m$^3$; and $X_x$ is the pollutant concentration measured by the sensor, also expressed in μg/m$^3$.

The concentration threshold values applied in the system are based on the ISPU breakpoints, as presented in Table 1.

Table 1. ISPU breakpoints for $PM_{10}$, $PM_{2.5}$, and CO

| Category | ISPU | $PM_{10}$ (μg/m$^3$) | $PM_{2.5}$ (μg/m$^3$) | CO (μg/m$^3$) |
|---|---|---|---|---|
| Good | 0-50 | 50 | 15.5 | 4000 |
| Moderate | 51-100 | 150 | 55.4 | 8000 |
| Unhealthy | 101-200 | 350 | 150.4 | 15000 |
| Very Unhealthy | 201-300 | 420 | 250.4 | 30000 |
| Hazardous | >300 | 500 | 500 | 45000 |

Using the breakpoint values, the system first identifies the pollutant-concentration interval that contains the measured value and then selects the corresponding upper and lower limits for interpolation. For instance, a $PM_{2.5}$ concentration of 33.6 µg/m³ falls within the 15.5 to 55.4 µg/m³ breakpoint range. Thus, (X_b = 15.5), (X_a = 55.4), (I_b = 50), and (I_a = 100). Applying linear interpolation gives a $PM_{2.5}$ subindex of 72.68, which is rounded to 73 and classified as Moderate. The overall ISPU category is assigned based on the highest subindex among $PM_{2.5}$, $PM_{10}$, and CO. The buzzer remains off for Good and Moderate conditions, produces one short beep for Unhealthy, two short beeps for Very Unhealthy, and a continuous alarm for Hazardous conditions.

### 2.6. Sensor Calibration and Accuracy Evaluation

Sensor performance was evaluated by co-locating the low-cost sensors with a reference instrument under identical test conditions. The paired observations were divided into two non-overlapping datasets: a calibration dataset used to estimate the calibration model and an independent validation dataset used only to assess performance. The same observation was therefore not used both to estimate a correction and to evaluate the corrected result. The reference instrument model, manufacturer, measurement range, stated accuracy, calibration status, number of paired observations in each dataset, sampling interval, co-location duration, and environmental conditions should be reported to support reproducibility.

$$Offset = Value_{referensi} - Value_{sensor} \tag{2}$$

For each pollutant parameter, a calibration model was fitted using the calibration dataset. For a linear correction model, the calibrated sensor value was calculated as: Value_calibrated = β0 + β1 × Value_sensor, where β0 is the fitted intercept and β1 is the fitted slope estimated exclusively from the calibration dataset. When temperature or relative humidity was included as a predictor, the model was specified as: Value_calibrated = β0 + β1 × Value_sensor + β2 × Temperature + β3 × RelativeHumidity. The coefficients were not derived from the corresponding validation observation. Model performance was then calculated on the independent validation dataset using mean absolute error (MAE), root-mean-square error (RMSE), mean bias, and, where appropriate, the Pearson correlation coefficient. If the available dataset was too small to create independent calibration and validation subsets, the authors should use blocked or k-fold cross-validation and report the procedure explicitly rather than applying a pair-specific offset.

$$Value_{calibration} = Value_{sensor} + Offset \tag{3}$$

For ISPU calculation, the calibrated CO concentration was converted from ppm to µg/m³ using: CO_µg/m³ = CO_ppm × MW × P / (R × T), where MW is the molecular weight of CO, P is pressure, R is the gas constant, and T is absolute temperature. If the analysis assumes 25 °C and 1 atm, this assumption must be stated and applied consistently. The calibration model and the ISPU classification should be evaluated on validation observations that were not used to estimate the calibration coefficients.

$$\mu g/m^3 = \frac{(ppm \times MW)}{(24.5 \times 10^{-3})} \tag{4}$$

In the CO concentration conversion equation, $CO_{ppm}$ denotes the carbon monoxide concentration expressed in parts per million (ppm), while MW represents the molecular weight of CO, which is 28.01 g/mol. The value 24.45 L/mol denotes the molar volume of an ideal gas at 25°C and 1 atm, whereas the factor $10^{-3}$ is used to convert liters to cubic meters. Accordingly, the equation converts CO concentration from ppm to µg/m³ under the stated temperature and pressure assumptions.

$$Error = \left| \frac{Value_{referensi} - Value_{sensor}}{Value_{referensi}} \right| x\ 100\% \tag{5}$$

The lower the Mean Relative Error (MRE) value, the better the sensor's measurement accuracy, because a smaller MRE indicates that the sensor readings are closer to the corresponding reference-instrument measurements across the validation dataset.

## 3. RESULTS AND DISCUSSION

### 3.1. Hardware Implementation

Figure 6. Implemented transmitter and receiver nodes

Figure 6 presents the implemented transmitter and receiver nodes of the proposed LoRa-based air-quality monitoring system. The transmitter node incorporates a ZH03B sensor for measuring $PM_1$, $PM_{2.5}$, and $PM_{10}$, a MiCS-5524 sensor for CO detection, and a DHT22 sensor for temperature and relative-humidity measurements. An ACS712 sensor is used to measure the transmitter current for power-consumption monitoring. The ESP32 processes the sensor data and sends the resulting packets to the receiver through the RFM95W LoRa module. The transmitter is powered by rechargeable Li-ion batteries supported by a TP4056 charging module, a battery-management system, an SX1308 step-up converter, and an LM7805 voltage regulator. The receiver node uses another ESP32 and RFM95W module to receive the data, display the measurements on a 16 × 2 $I_2C$ LCD, and store them locally on a microSD card. A voltmeter is used to monitor the receiver supply voltage, while a buzzer provides system-status indication and ISPU-based air-quality warnings.

### 3.2. Performance Assessment of the ZH03B Sensor

The ZH03B sensor estimates particulate-matter concentrations based on the laser light-scattering principle. Airborne particles passing through the sensing chamber scatter the laser beam, and the scattered light is detected by a photodetector and converted into PM concentration values in µg/m³. The performance of the ZH03B sensor was evaluated by comparing its readings with those obtained from a reference air-quality detector for $PM_1$, $PM_{2.5}$, and $PM_{10}$.

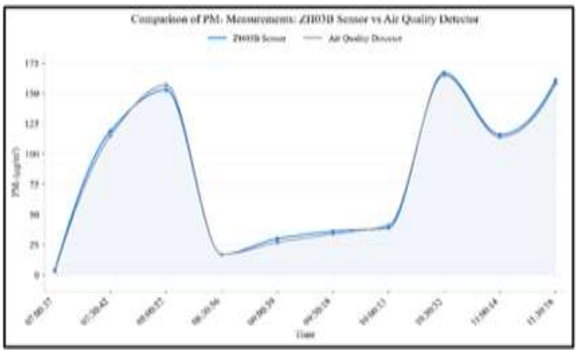


Figure 7. Comparison of $PM_1$ concentrations

Figure 7 compares $PM_1$ measurements recorded by the ZH03B sensor and the reference instrument. The ZH03B measured $PM_1$ concentrations ranging from 4 to 167 µg/m³, with an average error of 6.61% relative to the reference values. The lowest concentration was recorded at 07:00 a.m., whereas the highest value occurred at 10:30 a.m. Both measurement series showed similar temporal patterns during the observation period, suggesting that the ZH03B was able to track short-term $PM_1$ variations under the tested conditions. However, this agreement should be interpreted cautiously because the evaluation was based on a limited number of paired observations and did not include uncertainty quantification or statistical association analysis.

Figure 8 presents a comparison of $PM_{2.5}$ concentrations measured by the ZH03B sensor and the reference instrument. The ZH03B recorded $PM_{2.5}$ values between 6 and 179 µg/m³, with an average error of 10.58% relative to the reference measurements. Both datasets showed similar temporal trends, with the maximum concentration observed at 10:30 a.m. Based on the applied ISPU breakpoints, one observation was categorized as Good, four as Moderate, two as Unhealthy, and three as Very Unhealthy. These results show that $PM_{2.5}$ concentrations varied considerably during the observation period.

Figure 8. Comparison of $PM_{2.5}$ concentrations

Figure 9. Comparison of $PM_{10}$ concentrations

Figure 9 compares $PM_{10}$ concentrations obtained from the ZH03B sensor and the reference instrument. The ZH03B measured $PM_{10}$ values ranging from 10 to 197 µg/m³, with an average error of 8.67% relative to the reference values. The two-measurement series followed similar temporal patterns, and the highest concentration was recorded at 10:30 a.m. According to the stated ISPU breakpoints, three observations were classified as Good, four as Moderate, and three as Unhealthy. These findings indicate notable temporal variation in $PM_{10}$ concentrations during the observation period.

### 3.3. Performance Assessment of the MiCS-5524 Sensor

Figure 10. Comparison of CO concentrations

Figure 10 compares CO concentrations measured by the MiCS-5524 sensor with those recorded by the reference instrument. The MiCS-5524 measured CO values ranging from 0.82 to 9.3 ppm, with an average error of 18.48% relative to the reference measurements. The minimum concentration was recorded at 07:00 a.m., whereas the maximum value occurred at 11:00 a.m. Both datasets showed a generally increasing trend over the observation period, although deviations between the sensor and reference readings were observed at several time points. For ISPU classification, the corrected CO values were first converted from ppm to µg/m³ and then compared with the relevant breakpoint values. These results suggest that the MiCS-5524 can track short-term CO variations, but its relatively high average error indicates the need for improved calibration and further validation.

### 3.4. Performance Assessment of the DHT22 Sensor

Figure 11. Comparison of air-temperature measurements

Figure 11 presents a comparison of air-temperature measurements obtained from the DHT22 sensor and the reference instrument. The DHT22 recorded temperatures between 27.7 and 37.0°C, while the reference instrument measured values from 27.4 to 37.2°C. The mean relative errors of 0.87%, indicating close agreement between the two datasets under the tested conditions. Air temperature generally increased from morning to midday, reached its maximum value of 37.0°C at 11:00 a.m., and then decreased to 34.3°C at the final observation. Further statistical analysis is needed to evaluate the relationship between temperature, relative humidity, and pollutant concentrations.

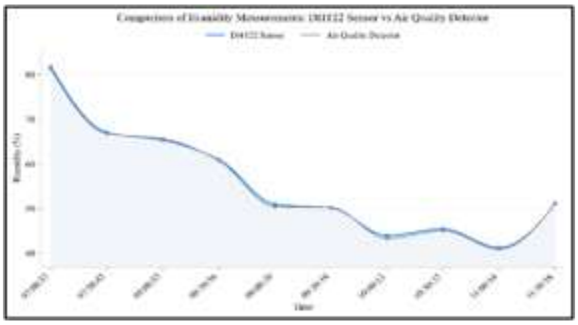

Figure 12. Comparison of relative humidity measurements

Figure 12 shows a comparison of relative-humidity measurements recorded by the DHT22 sensor and the reference instrument. The DHT22 measured relative humidity values from 41.2% to 81.7%, while the reference instrument recorded values between 40.9% and 81.2%. The mean relative errors of 0.61%, showing close agreement between the two datasets under the tested conditions. Relative humidity generally declined from the morning period, reached its lowest value of 41.2% around midday, and then increased to approximately 51% at the final observation. Additional statistical analysis is needed to clarify the relationships among relative humidity, temperature, and pollutant concentrations.

### 3.5. LoRa Communication Performance Assessment

The performance of the LoRa communication link was evaluated under Line-of-Sight (LoS) and Non-Line-of-Sight (Non-LoS) conditions by transmitting 121-byte data packets at predefined distances and measuring packet loss, end-to-end delay, jitter, and throughput.

#### 3.5.1. Line of Sight (LoS)

Table 2 indicates that LoRa communication performance declined as the transmission distance increased under LoS conditions. Up to 1,200 m, all transmitted packets were successfully received, resulting in 0% packet loss and relatively stable throughput between 233.3 and 239.4 bps. Within this range, the average delay rose from 201 to 697 ms, while jitter varied across distances but increased overall from 10 to 33.75 ms. At 1,400 m, packet loss increased sharply to 58.33%, meaning that only five of twelve transmitted packets were received. At this distance, the average delay and jitter increased to 1,408 and 355 ms, respectively, while throughput dropped to 102.5 bps. No packets were received at 1,500 m. These findings show that the LoRa link remained reliable up to 1,200 m under the tested LoS conditions, but communication quality deteriorated substantially at 1,400 m.

Table 2. LoRa communication performance under Line-of-Sight conditions

| Distance (m) | Packet Loss (%) | Avg. Delay (ms) | Jitter (ms) | Throughput (bps) |
|---|---|---|---|---|
| 50 | 0 | 201 | 10 | 239.4 |
| 100 | 0 | 242 | 18.75 | 239 |
| 200 | 0 | 282 | 26.25 | 238.6 |
| 400 | 0 | 322 | 16.25 | 238.3 |
| 600 | 0 | 368 | 23.75 | 237.5 |
| 800 | 0 | 464 | 23.75 | 236.5 |
| 1000 | 0 | 565 | 26.25 | 235.1 |
| 1200 | 0 | 697 | 33.75 | 233.3 |
| 1400 | 58.33 | 1408 | 355 | 102.5 |
| 1500 | Data not received | | | |

### 3.5.2. Non-Line of Sight (NLoS)

Table 3. LoRa testing under non-line of sight conditions

| Distance (m) | Packet Loss (%) | Avg. Delay (ms) | Jitter (ms) | Throughput (bps) |
|---|---|---|---|---|
| 5 | 0 | 207 | 15 | 239.2 |
| 10 | 0 | 252 | 15 | 238.8 |
| 20 | 0 | 434 | 52.5 | 236.4 |
| 30 | 44.44 | 558 | 75 | 234.7 |
| 40 | 50 | 706 | 98.75 | 118.3 |
| 50 | 58.33 | 1140 | 112.5 | 116.9 |
| 60 | Data not received | | | |

Table 3 indicates that LoRa communication performance decreased as distance increased under Non-Line-of-Sight conditions. Packet transmission remained fully successful up to 20 m, with 0% packet loss and throughput values between 236.4 and 239.2 bps. Within this range, the average delay increased from 207 to 434 ms, and jitter rose from 15 to 52.5 ms. At 30 m, packet loss reached 44.44%, while the average delay and jitter increased to 558 and 75 ms, respectively. Further degradation was observed at 40 m, where packet loss reached 50%, average delay increased to 706 ms, jitter reached 98.75 ms, and throughput dropped to 118.3 bps. At 50 m, packet loss increased to 58.33%, with an average delay of 1,140 ms, jitter of 112.5 ms, and throughput of 116.9 bps. No packets were received at 60 m. These results show that loss-free communication was maintained only up to 20 m under the tested Non-LoS conditions.

### 3.6. Web ServerPerformance Assessment

The web-server functionality test evaluated whether the proposed system could receive, store, and display air-quality monitoring data. The results showed that measurements sent from the receiver node were successfully stored in the Firebase Realtime Database and displayed on the online dashboard. The dashboard presented key environmental parameters, including temperature, relative humidity, $PM_1$, $PM_{2.5}$, $PM_{10}$, and CO, enabling remote observation of air-quality conditions at the monitoring site.


Figure 13. Web-server interface for real-time monitoring

Figure 13 presents the Firebase Realtime Database and web-dashboard interfaces used in the monitoring system. The sensor data were successfully recorded in the database and displayed on the dashboard, demonstrating end-to-end data transfer from the receiver node to the monitoring interface.

### 3.7. Air Quality Sensor Data Trend Analysis

Table 4. Seven-day field measurements and ISPU categories

| Date | Temperature ($^0$C) | Humidity (%) | $PM_{2.5}$ (µg/m³) | CO (ppm) |
|---|---|---|---|---|
| 12 Mei 2026 | 32.7 | 59 | 75 | 4.89 |
| 13 Mei 2026 | 32.4 | 60.6 | 60 | 2.01 |
| 14 Mei 2026 | 34.9 | 50 | 103 | 4.68 |
| 15 Mei 2026 | 29 | 74.5 | 46 | 2.84 |
| 16 Mei 2026 | 31.7 | 63.5 | 49 | 4.21 |
| 17 Mei 2026 | 29.1 | 74.3 | 28 | 1.45 |
| 18 Mei 2026 | 30.3 | 69.4 | 85 | 3.90 |

Table 4 summarizes the daily average temperature, relative humidity, $PM_{2.5}$ concentration, and CO concentration recorded during the seven-day field deployment. Temperature ranged from 29.0 to 34.9°C, while relative humidity ranged from 50.0% to 74.5%. The highest temperature and lowest relative humidity were recorded on 14 May 2026, whereas the lowest temperature and highest relative humidity were observed on 15 May 2026. These results indicate temporal variation in environmental conditions during the monitoring period, although a statistical test is required to confirm any relationship between temperature and relative humidity.

Daily average $PM_{2.5}$ concentrations ranged from 28 to 103 µg/m³. Based on the applied ISPU breakpoints, $PM_{2.5}$ concentrations on 15, 16, and 17 May were classified as Moderate, while those on 12, 13, 14, and 18 May were classified as Unhealthy. The lowest $PM_{2.5}$ concentration was recorded on 17 May 2026, whereas the highest value occurred on 14 May 2026. These findings show that $PM_{2.5}$ was the dominant pollutant affecting the daily air-quality category during the observation period. CO concentrations ranged from 1.45 to 4.89 ppm. The lowest CO concentration was recorded on 17 May 2026, while the highest value occurred on 12 May 2026. For ISPU classification, CO concentrations were first converted from ppm to µg/m³. The converted CO values were classified as Good on 13, 15, and 17 May, and Moderate on 12, 14, 16, and 18 May. Overall, 17 May showed the lowest $PM_{2.5}$ and CO concentrations, while 14 May recorded the highest $PM_{2.5}$ concentration. Because the dataset covers only seven days, further statistical analysis is needed before drawing conclusions about relationships among temperature, relative humidity, $PM_{2.5}$, and CO.

## 4. CONCLUSION

The proposed system was successfully implemented to monitor $PM_1$, $PM_{2.5}$, $PM_{10}$, CO, temperature, and relative humidity through a web dashboard, LCD, local microSD storage, and an ISPU-based early-warning mechanism. The system determines the overall air-quality category from the highest ISPU subindex for $PM_{2.5}$, $PM_{10}$, and CO and activates the corresponding warning signal when the category reaches Unhealthy or higher. Sensor evaluation showed mean relative errors of 6.61%, 10.58%, and 8.67% for $PM_1$, $PM_{2.5}$, and $PM_{10}$, respectively, using the ZH03B sensor; the MiCS-5524 sensor showed a mean relative error of 18.48% for CO, while the DHT22 showed mean relative errors of 0.87% for temperature and 0.61% for relative humidity. LoRa communication achieved 0% packet loss up to 1,200 m under LoS conditions and up to 20 m under the tested NLoS conditions. During the seven-day deployment, the highest daily mean $PM_{2.5}$ concentration was recorded on 14 May 2026 and classified as Unhealthy, demonstrating the system's ability to identify degraded air-quality conditions and provide an early warning. These findings support the technical feasibility of the proposed platform for short-term indicative monitoring and local early warning in sand-mining areas, although they do not establish regulatory equivalence. Future work should include longer deployments, additional monitoring points, independent validation of the warning response, improved CO calibration, LoRa parameter optimization, and more comprehensive evaluation of air-quality warning performance.

## ACKNOWLEDGEMENTS

The authors sincerely thank the Head of the Electronics Laboratory, Department of Electrical Engineering, Tadulako University, for providing the facilities, technical resources, and support needed for the design, development, and experimental evaluation of the proposed system. The authors also express their appreciation to the research team and students for their valuable assistance in completing this study and preparing the manuscript.

## REFERENCES

[1] Z. Deng, D. Weng, J. Chen, R. Liu, Z. Wang, and J. Bao, "AirVis: visual analytics of air pollution propagation," *IEEE Transactions on Visualization and Computer Graphics*, vol. 26, no. 1, pp. 800 - 810, Jan. 2020, doi: 10.1109/TVCG.2019.2934670.
[2] J, Kumaran and S. Mohan, "A review on air pollution prediction using artificial intelligence," *IEEE Access*, vol. 14, pp. 26024-26040, Feb. 2026, doi: 10.1109/ACCESS.2026.3664880.
[3] J. Kalajdjieski, K. Trivodaliev, G. Mirceva, S. Kalajdziski, and S. Gievska, "A complete air pollution monitoring and prediction framework," *IEEE Access*, vol. 11, pp. 88730 - 88744, Mar. 2023, doi: 10.1109/ACCESS.2023.3251346.
[4] S. Jiyal, J. Sheetlani, and R. K. Saini, "Internet of things: a survey on air pollution monitoring, challenges and applications," *in Proc. IEEE International Conference on Computing, Communication and Security (ICCCS)*, Mar. 2023, doi: 10.1109/ICCCS55188.2022.10079635.
[5] S. Jiyal and R. K. Saini, "Prediction and monitoring of air pollution using internet of things (IoT)," *in Proc. IEEE International Conference on Parallel, Distributed and Grid Computing (PDGC)*, Jan. 2021, doi:10.1109/PDGC50313.2020.9315831.
[6] J. M. García, E. R. Sorroche, S. B. Díaz, G. G. Contreras, and A. Muñoz, "Reducing pollution health impact with air quality prediction assisted by mobility data," *IEEE Journal of Biomedical and Health Informatics*, vol. 29, no. 12, pp. 9210- 9220, Dec. 2025, doi: 10.1109/JBHI.2024.3508466.
[7] W. Loungon, T. Kreetachat, S. Imman, N. Suriyachai, S. Wongcharee, and P. Thanarat, "Enhancing air quality with an innovative IoT-integrated hybrid air pollution control system," *IEEE Geoinformatics for Spatial-Infrastructure Development in Earth and Allied Sciences (GIS-IDEAS)*, May 2025, doi: 10.1109/GIS-IDEAS63212.2024.10990965.
[8] B. Sudantha, M. Manchanayaka, C. Yang, C. Premachandra, M. Firdhous, and K. Sumathipala, "IoT empowered open sensor network for environmental air pollution monitoring system in smart cities," *in Proc. IEEE International Conference on Information Technology Research (ICITR)*, Jan. 2024, doi: 10.1109/ICITR61062.2023.10382893.
[9] J. Pellegrino, H. Aziza, M. Guerin, P. Taranto, W. Rahajandraibe, and B. Ravelo, "Development of a multi-sensor mobile device for urban air quality monitoring at the street corner: the smile project," *IEEE Access*, vol. 13, pp. 14857-14871, Jan. 2025, doi: 10.1109/ACCESS.2025.3530145.
[10] A. B. Satriobudi, Iskandar, and A. Mustafa, "IoT prototype air quality monitoring using lora communication system on frequency 433 Mhz," *in Proc. IEEE International Conference on Telecommunication Systems, Services, and Applications (TSSA)*, Mar. 2023, doi:10.1109/TSSA56819.2022.10063914.
[11] M. A. Izzulhaq, R. T. Widodo, and H. Oktavianto, "LoRa-Based IoT recommendations for surabaya city drainage channel using multi-node multi-hop communication," *Jurnal Rekayasa Elektrika*, vol. 21, no. 2, pp. 52-63, Jun. 2025, doi: 10.17529/jre.v21i2.45095.
[12] V. Rujivorakul and S. Vorapatratorn, "Online low-cost air quality monitoring system using lora-based communication," *in Proc. IEEE International Joint Conference on Computer Science and Software Engineering (JCSSE)*, Aug. 2024, doi:10.1109/JCSSE61278.2024.10613672
[13] G. Vicente and G. Marques, "Air quality monitoring through LoRa technologies: a literature review," *in Proc. IEEE International Conference on Decision Aid Sciences and Application (DASA)*, Jan. 2021, doi:10.1109/DASA51403.2020.9317300.
[14] H. Yu and I. Zahidi, "Environmental hazards posed by mine dust, and monitoring method of mine dust pollution using remote sensing technologies: an overview," *Science of The Total Environment*, vol. 864, Mar. 2023, doi:10.1016/j.scitotenv.2022.161135.
[15] Z. Wang, W. Zhou, I. M. Jiskani, H. Luo, Z. Ao, and E. M. Mvula, "Annual dust pollution characteristics and its prevention and control for environmental protection in surface mines," *Science of The Total Environment*, vol. 825, Jun. 2022, doi: 10.1016/j.scitotenv.2022.153949.
[16] M. Sofyan, "Persepsi masyarakat penambang pasir dan batu terhadap kondisi lingkungan dan tata kelola penambangan di Kelurahan Watusampu Kecamatan Palu Barat Kota Palu Propinsi Sulawesi Tengah," M.S. thesis, Department of Environmental Science, Universitas Gadjah Mada, Yogyakarta, Indonesia, 2007. [Online]. Available: https://etd.repository.ugm.ac.id/penelitian/detail/35971.
[17] P. J. Kute, Z. Zeffitni, and M. Marjan, "Analisis penurunan kualitas udara parameter PM2.5 dan PM10 akibat dari aktivitas tambang bahan galian C di Jalan Trans Palu–Donggala," Sarjana thesis, Universitas Tadulako, Palu, Indonesia, 2023. [Online]. Available: https://repository.untad.ac.id/id/eprint/105359/.
[18] N. I. Risqi, "Evaluasi kualitas udara partikulat matter (PM2.5 dan PM10) pada Puskesmas Pembantu Watusampu di Kota Palu," Sarjana thesis, Universitas Tadulako, Palu, Indonesia, 2026. [Online]. Available: https://repository.untad.ac.id/id/eprint/155562/.
[19] F. Carotenuto, A. Bisignano, L. Brilli, G. Gualtieri, and L. Giovannini, "Low-cost air quality monitoring networks for long-term field campaigns: A review," Meteorological Applications, 2023, doi: 10.1002/met.2161.
[20] M. R. Giordano et al., "From low-cost sensors to high-quality data: A summary of challenges and best practices for effectively calibrating low-cost particulate matter mass sensors," Journal of Aerosol Science, vol. 153, 2021, art. no. 105833, doi: 10.1016/j.jaerosci.2021.105833.
[21] P. deSouza et al., "Calibrating networks of low-cost air quality sensors," Atmospheric Measurement Techniques, vol. 15, pp. 6309–6331, 2022, doi: 10.5194/amt-15-6309-2022.
[22] F. Concas et al., "Low-Cost Outdoor Air Quality Monitoring and Sensor Calibration," ACM Transactions on Sensor Networks, vol. 17, no. 2, 2021, doi: 10.1145/3446005.
[23] F. Concas et al., "Low-Cost Outdoor Air Quality Monitoring and Sensor Calibration," ACM Transactions on Sensor Networks, vol. 17, no. 2, 2021, doi: 10.1145/3446005.
[24] M. L. Zamora, C. Buehler, A. Datta, D. R. Gentner, and K. Koehler, "Identifying optimal co-location calibration periods for low-cost sensors," Atmospheric Measurement Techniques, vol. 16, pp. 169–184, 2023, doi: 10.5194/amt-16-169-2023.
[25] K. K. Barkjohn et al., "Air Quality Sensor Experts Convene: Current Quality Assurance Considerations for Credible Data," ACS ES&T Air, vol. 1, no. 10, 2024, doi: 10.1021/acsestair.4c00125.
[26[ M. A. Sulimat and N. Katiran, "IoT based air quality monitoring system using LoRaWAN," Evolution in Electrical and Electronic Engineering, vol. 5, no. 2, pp. 116-125, Oct. 2024, doi:10.30880/eeee.2024.05.02.014.